THE JOURNAL OF PHYSICAL CHEMISTRY B

Article

Cite This: J. Phys. Chem. B 2019, 123, 6643−6650

pubs.acs.org/JPCB

Mueller Tensor Nonlinear Optical Polarization Analysis in Turbid Media

Published as part of The Journal of Physical Chemistry virtual special issue "Hai-Lung Dai Festschrift".

James R.W. Ulcickas and Garth J. Simpson*

Department of Chemistry, Purdue University, 560 Oval Drive, West Lafayette, Indiana 47906, United States

ABSTRACT: A mathematical framework to treat partial polarization in second harmonic generation imaging of nonlinear optical susceptibility is described and applied to imaging tissue sections 5, 40, and 70 μm thick, sufficient to introduce significant depolarization of the incident field. Polarization analysis becomes complicated in turbid media, in which scattering can result in degradation of polarization purity. The simplest framework for describing the polarization of purely polarized light is the Jones framework, which has been applied to great effect in the polarization analysis of second harmonic generation. However, the Jones framework lacks the necessary generality to describe a partially polarized electric field, (i.e., ones positioned within the volume of the Poincaré sphere rather than on the surface). Recent work connecting the Jones framework to the Mueller−Stokes framework has enabled interpretation of results with the more intuitive Jones framework while maintaining generality of the Mueller−Stokes method. The magnitude and nature of linear interactions of the tissue with the incident infrared field are discussed. Despite substantial depolarization, the nonlinear optical susceptibility tensor elements of collagen was recoverable at each pixel images of thick tissue utilizing the described framework. For thick and thin tissues, values of the tensor element ratio ρ were recovered in good agreement with previous studies. Both hyperpolarizing and depolarizing effects of SHG were observed, and the mechanism of hyperpolarization was determined to rest upon the interplay of orientation and relative contribution of polarized and depolarized incident light to elicit SHG.

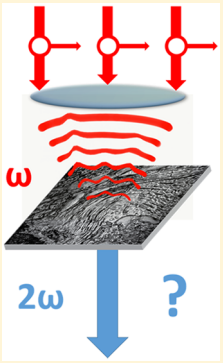

INTRODUCTION

Nonlinear optical microscopies including second harmonic generation (SHG) and two-photon excited fluorescence (TPEF) provide high contrast within turbid media, supporting analysis of biologically relevant systems. The quadratic power dependence of signal on the incident intensity generally confines the emitted signal to the focal plane, enabling optical sectioning without confocal detection. The ability to use near-infrared (IR) incident light further reduces scattering losses for imaging deeply within biological structures, i.e., tissue samples. Endogenous expression of mutants hybridized with fluorescent proteins has lent itself to imaging a variety of protein targets, including mBlueberry1, EGFP, and mCherry, among others, as well as its use with Ca^{2+} binding fluorescent tags for monitoring neural activity.[1,2] The intrinsic fluorescence of aromatic amino acid residues has enabled its routine use in *in vivo* imaging of microvasculature, as well as NADH metabolism.[3,4] While the generality of TPEF makes it a flexible imaging modality for biologically relevant systems, SHG provides a symmetry specific contrast mechanism with lower background without the need for labeling. The selection rules for SHG necessitate a noncentrosymmetric structure, as can be found in the form of collagen networks in the extracellular matrix and myosin assemblies in muscle fibers. SHG has been employed to study the organization of collagen, which has been previously demonstrated to correlate with expression of several diseases, including lung, ovarian, and breast cancers.[5−7]

Polarization dependence allows the expansion of these methods to unique chemical problems; for example, polarization-resolved TPEF has been utilized previously to distinguish amorphous from crystalline proteins in the field of structural biology.[8] Polarization-resolved SHG has been utilized to image biological structures such as collagen and myosin while obtaining information about molecular organization.[9,10] Collagen is the primary structural element of the extracellular matrix, composed of a supramolecular assembly of collagen triple helices oriented uniaxially to form a fibril, with many fibrils contained in a single fiber. The relative orientation of collagen triple helices with respect to the fibril axis and, consequently, the fiber axis dictates the relative contribution of the molecular hyperpolarizability to the NLO susceptibility tensor. It has previously been demonstrated that the local order, i.e., distribution of triple helix tilt angles with respect to fiber axis, is altered with pathological expression of certain disease states and can thus be probed by polarization sensitive SHG microscopy.[5,6,11]

Despite the clear benefits of polarization analysis in SHG and TPEF microscopy, implementation in vivo is frustrated by turbidity and birefringence, which complicate polarization analysis in multiple ways. In the case of both protein crystal imaging and thick tissue imaging, the sample plane may lie

Received: May 24, 2019
Revised: July 9, 2019
Published: July 10, 2019

DOI: 10.1021/acs.jpcb.9b04961
J. Phys. Chem. B 2019, 123, 6643−6650

embedded within the scattering medium. Thus, propagation of light to the sample plane may cause depolarization to occur prior to SHG due to mixing of polarization states. Furthermore, for backscattering imaging geometries or cases where the nonlinear signal must propagate through a substantial path length of tissue prior to detection, the SHG can be further depolarized. Several methods have been developed to combat this complication. In 2010, Schanne-Kleine and co-workers utilized simultaneous detection of backscattered and transmitted SHG and fundamental beams to quantify the interplay between birefringence and collagen structure; however, this work did not address the effect of homogeneous scattering.[12] More recently, adaptive optics and phase-only wavefront shaping have been employed to shape the polarization of the incident light to deliver pure polarizations at the sample plane beneath turbid media to account for scattering occurring prior to SHG.[13]

Alternative methods utilize theoretical modeling to predict NLO signal in the presence of depolarization, such that changes in polarization due to structure of the NLO susceptibility tensor may be disentangled from scattering and birefringence effects upon the incident beam. The classical Jones framework to describe linear, and more recently, nonlinear optics is insufficient to describe the polarization state of partially polarized light. To account for this deficiency, Shi, McClain, and Harris extended the more general Stokes–Mueller framework to nonlinear optics.[14,15] Recent efforts by Barzda have extended these theoretical models to account for depolarization induced by the sample during measurement with the double Mueller matrix approach, which has been applied to studies of collagen.[16,17] Recently, a complementary framework was developed by Simpson and co-workers, connecting the intuitive Jones framework to the more general Stokes framework.[18] This latter Mueller tensor framework provides the means to bridge measured Stokes vectors with the Jones tensor describing the NLO susceptibility. The complexity of the vectorized tensor determining SHG activity is thus reduced from 64 in the Mueller framework to 8 in the Jones framework. We have demonstrated the validity of the Jones/Mueller framework in the limit of a completely depolarized fundamental, showing excellent predictive capacity for the model system of Z-cut quartz and enabling the recovery of the tensor element ratio ρ as well as orientation of collagen fibers in a thin tissue section of mouse tail.[19]

The work detailed herein utilizes the Mueller tensor framework for recovering structural information from SHG microscopy in thick tissue sections, where depolarization is significant. SHG produced from collagen embedded in 5, 40, and 70 μm thick mouse tail tendon sections was measured and its polarization analyzed via a rotating quarter wave plate (QWP) and wire grid polarizer. As light propagates to the focal plane through the tissue, scattering and birefringence alter the incident polarization and mix the orthogonal polarization components. Fitting to recover the Stokes vectors describing polarization of the fundamental and second harmonic enables the recovery of Jones tensor elements through the Mueller tensor mathematical framework. Full tensor element images were obtained for χ_{zzz} and χ_{zxx}, enabling recovery of the tensor element ratio $\rho = \chi_{zzz}/\chi_{zxx}$. This ratio offers a measure of molecular-scale disorder within the collagen fiber, which can act as a quantitative probe to changes in extracellular structure associated with expression of pathologies such as lung, breast, and ovarian cancers.[5−7] Images of ρ for collagen embedded in thick tissue showed good agreement with previous measurements of mouse tail tendon in thin sections.

THEORETICAL FOUNDATION

The Jones formalism describes the polarization state of an electric field in a basis set of the two orthogonal field components, most commonly horizontal and vertical or more generally transverse electric and transverse magnetic. Equation 1 below indicates the general form for a Jones vector and the application of a linear optical process by matrix multiplication, i.e., interaction with a generalized nondepolarizing optical element represented by the 2 × 2 Jones matrix J.

$$\vec{e}_{out} = J \cdot \vec{e}_{in} \tag{1}$$

In contrast, the Stokes vector describes polarization through a four element vector, in which each element is determined by the relative intensity of different polarization components. The first element contains the total integrated intensity, such that a normalized Stokes vector has a first element equal to 1. Equation 2 below defines the Stokes vector $\vec{s}$, and relates it to the Jones vector $\vec{e}$. Intensity information is obtained by the Kronecker product of the field components, in combination with the transfer matrix A, which maps those intensities in appropriate combination to the elements of $\vec{s}$. Note that the definition of $\vec{s}$ is such that unpolarized light is described by the Stokes vector $\vec{s} = [1\,0\,0\,0]^{T}$.

$$\vec{s} = \begin{pmatrix} I_H + I_V \\ I_H - I_V \\ I_{+45} - I_{-45} \\ I_R - I_L \end{pmatrix} = \begin{bmatrix} 1 & 0 & 0 & 1 \\ 1 & 0 & 0 & -1 \\ 0 & 1 & 1 & 0 \\ 0 & i & -i & 0 \end{bmatrix} \cdot \begin{pmatrix} \vec{e}_H^{*}\vec{e}_H \\ \vec{e}_H^{*}\vec{e}_H \\ \vec{e}_V^{*}\vec{e}_H \\ \vec{e}_V^{*}\vec{e}_V \end{pmatrix}$$

$$= A \cdot (\vec{e}^{*} \otimes \vec{e}) \tag{2}$$

In much the same way that nondepolarizing optical components can be represented by Jones matrices in the Jones framework, the Stokes framework utilizes Mueller matrices M to indicate linear processes that can include partial or complete depolarization. The Mueller matrix for any generalized nondepolarizing optical element can again be constructed from the Jones matrix for that same optic in combination with the transfer matrix A.

$$\vec{s}_{out} = A \cdot (J^{*} \otimes J) \cdot A^{-1} \cdot \vec{s}_{in} = M \cdot \vec{s}_{in} \tag{3}$$

For quadratic nonlinear processes such as SHG or TPEF, the output polarization and amplitude are functions of two input fields, and not one. As a result, propagating polarization in the Jones framework for these systems is most intuitively represented by the tensor product of the incident fields with the NLO susceptibility $\chi_J^{(2)}$. Once again, an analogous Mueller tensor, $M^{(2)}$, can be constructed utilizing the transfer matrix A and the corresponding Jones tensor.[18] The Jones tensor, $\chi_J^{(2)}$, is formally a 2 × 2 × 2 tensor in the laboratory reference frame, while $M^{(2)}$ is a 4 × 4 × 4. The mapping between Jones and Mueller tensors represented in Equation 4 below allows the generality of the Stokes–Mueller framework to be employed for compatibility with partially depolarized incident light, with simpler interpretation afforded by the Jones framework.

$$M^{(2)} = A \cdot (\chi_J^{(2)*} \otimes \chi_J^{(2)}) : A^{-1}A^{-1} \tag{4}$$

DOI: 10.1021/acs.jpcb.9b04961
J. Phys. Chem. B 2019, 123, 6643−6650

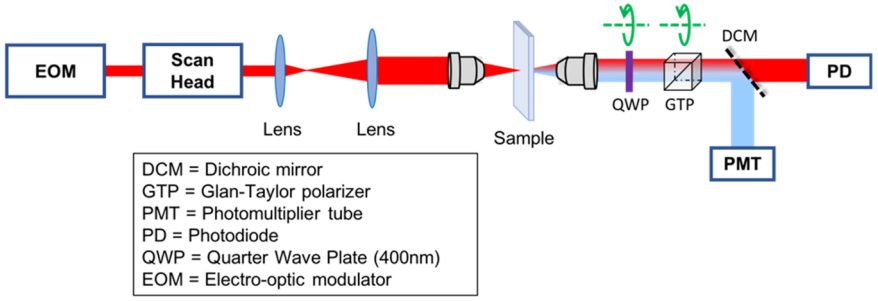

Figure 1. Instrument schematic. 800 nm light from an 80 MHz pulsed Ti sapphire propagates through an EOM operating at 8 MHz, generating 10 unique polarization states. The scan head rasters the beam across the field of view, while a rotating QWP and polarizer serve as the analyzer for Stokes vector evaluation.

Equation 4 holds provided that the NLO process itself is intrinsically nondepolarizing, in which case the Mueller tensor $M^{(2)}$ allows prediction of the partially polarized state of the SHG produced by partially polarized incident light. The validity of this framework has been supported previously utilizing SHG measurements of *Z*-cut quartz and thin collagen sections.[19] It was shown that for fully depolarized incident fields, resultant SHG followed intensity trends predicted by the Stokes–Mueller framework.

The theoretical treatment underpinning eqs 1–4 assumes that the measurement of the second harmonic is in the same reference frame as the harmonophore. In practice, this is not necessarily the case. A reference frame rotation is often included to connect the incident field in the laboratory frame to the local frame, followed by subsequent rotation from the local frame back to the laboratory frame. This procedure is done in the Jones framework by multiplication of 2 × 2 Jones rotation matrices R_ϕ, and analogous 4 × 4 Mueller rotation matrices $\mathcal{R}_\phi$ may be produced following the procedure described in eq 3. Equation 5 below connects the observed laboratory frame (indicated by the subscript "*L*") Stokes vectors to the local frame (indicated by the subscript "*l*") Mueller tensor $M_l^{(2)}$, which can be connected to the underlying Jones tensor through eq 4. Measured Stokes vectors for the fundamental and second harmonic enable recovery of Jones tensor elements by fitting to eq 5.

$$\vec{s}^{2\omega} = M_L^{(2)} : \vec{s}^{\omega}\vec{s}^{\omega} = \mathcal{R}_{-\phi} M_l^{(2)} : (\mathcal{R}_\phi \vec{s}^{\omega})(\mathcal{R}_\phi \vec{s}^{\omega}) \quad (5)$$

Note that while the mathematical framework formally incorporates all three Euler angles to describe the reference frame rotation from laboratory to local frames, for the specific case of collagen accounting for ψ is unnecessary due to cylindrical symmetry. Furthermore, due to the mouse tail sectioning approach utilized where tissue segments were taken parallel to the primary axis of tendon fibers, θ is assumed to be negligible.

METHODS

Figure 1 illustrates the experimental apparatus. Polarization resolved SHG microscopy was conducted by modulating incident polarization with an electro-optic modulator (EOM) and analyzing the exiting polarization via combination of a quarter wave plate (QWP) and polarizer. For a given incident polarization state, the QWP was rotated from 0° to 45° in 22.5° increments, while the polarizer was rotated from 0° to 135° in 45° increments, yielding 12 total measurements. The recorded intensity vector for each pixel was linearly fit to recover the Stokes vector for both the transmitted IR as measured on the photodiode, as well as the SHG intensity on the PMT. The EOM operating at 8 MHz (synchronously clocked to the IR light source, a pulsed 80 MHz Ti sapphire at 800 nm) yielded precisely 10 unique polarization states for the incident field, independently interrogated by synchronizing the EOM with the laser and the digital oscilloscope card as described previously.[20] The 10 separate polarizations allowed an overdetermined fit to recover local frame tensor elements of the sample at every signal-carrying pixel within the field of view.

Mouse tail samples were obtained from the laboratory of Prof. Philip Low (Purdue University, West Lafayette, IN) and fixed in 10% neutral buffered formaline. The tail was subsequently decalcified in solution of Formical-4 (StatLab) for 5 h, then placed in a 15% sucrose solution in PBS overnight, followed by a 30% sucrose solution in phosphate buffered saline overnight for cryoprotection. The use of sucrose for cryoprotection in preparing these tissue samples may have the secondary effect of acting as an index-matching medium, reducing the scattering measured within these samples relative to measurement of untreated tissue. Despite this, significant depolarization and birefringence were still observed, representing a lower bound for the degree of turbidity expected in untreated tissue. The tails were then embedded in optimal cutting temperature compound (OCT) and frozen using isopentane chilled with liquid nitrogen. Tissue sections were taken from the central region of the tail, cut longitudinally using a Leica CM 1860 cryostat. Cryosectioning full thick tissue segments enabled measurement of collagen fibers in their natural environment relative to other structures in the tissue. When imaging, the beam was focused on the rear plane of the sample, such that SHG produced underwent minimal Rayleigh scattering prior to collection. This approach simplified polarization analysis as all depolarization was reasonably assumed to occur on the incident light only. Prior to polarization analysis, the resulting images were blurred with a Gaussian filter (σ = 2) for signal averaging with adjacent pixels.

For each pixel in the 12 collected images, a vector of intensities was used to conduct a linear fit to the Stokes vector using eq 6 below, where γ is the angle between the laboratory frame and the fast axis of the wave plate, and ϕ_{pol} is the angle of the fast axis of the polarizer relative to the laboratory frame. The fit matrix **F** was constructed from the known Mueller matrices for the detection QWP and polarizer. In principal, the Stokes vector can be constructed from direct measurement of I_H, I_V, I_{+45}, I_{-45}, I_R, and I_L. In practice, a single wave plate was

DOI: 10.1021/acs.jpcb.9b04961
J. Phys. Chem. B 2019, 123, 6643–6650

used for both the 400 and 800 nm light; thus, the fundamental wavelength was not probed directly for I_R and I_L. Regardless, the right and left elliptical components were measured, which may be considered as a superposition of I_R and $I_L$with linearly polarized light, and enabled recovery of the Stokes vector by constructing the fit matrix with the appropriate phase retarder Mueller matrix.

$$I_{\text{det}} = [1 \quad 0 \quad 0 \quad 0]\cdot M_{pol}\cdot\mathcal{R}(\phi_{pol})\cdot\mathcal{R}(-\gamma)\cdot M_{WP}\cdot\mathcal{R}(\gamma)\cdot\vec{s}_{out} = F_{\gamma,\phi_{pol}}\cdot\vec{s}_{out} \tag{6}$$

For each of the 10 incident polarization states, 12 images were acquired as illustrated in Figure 2, corresponding to four

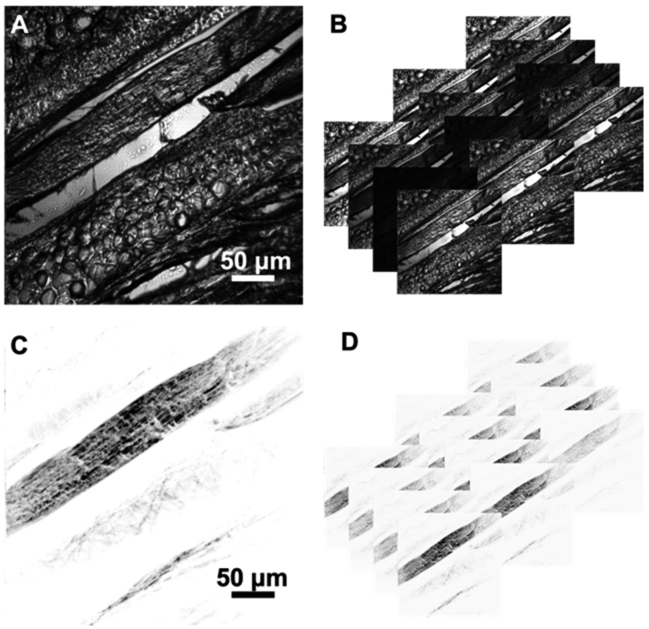

Figure 2. Images display total integrated intensity across all polarizations and analyzer configurations of laser transmittance (A) and SHG (C) for 40 m thick tissue. Stack of 12 images acquired with different analyzer configurations for polarization 1 for laser transmittance (B) and SHG (D).

unique polarizer angles and three unique quarter wave plate angles for the detection optics. For a single pixel, stacking each intensity from the unique analyzer configurations into a single vector expanded the dimensionality of the linear transform F in eq 6 above from a 1 × 4 to a 12 × 4 matrix, $\mathbf{F}$ in eq 7 below.

$$I_{\text{det}} = \mathbf{F}\vec{s}_{out};\quad \vec{s}_{out} = (\mathbf{F}^T\mathbf{F})\mathbf{F}^T I_{\text{det}} \tag{7}$$

Figure 2, above, shows the total integrated intensity of detected laser transmittance (A) and SHG (C) and the 12 unique images for polarization 1 (B, D) for 40 μm thick tissue. For both SHG and laser transmittance, a per-pixel linear fit was conducted to eq 6, reducing the set of 120 input images to 40 images corresponding to the Stokes vector elements for each of the 10 polarization states. This process was performed for both the transmitted infrared beam and the frequency doubled SHG light.

RESULTS AND DISCUSSION

Figure 3 shows the total integrated laser transmittance intensity for each of the three tissue thicknesses measured and demonstrates broadening of the distribution of degree of polarization (DoP) for pixels used in the polarization analysis. DoP is defined as DoP $= \sqrt{s_1^2 + s_2^2 + s_3^2}/s_0$. Tissue samples contain many refractive index changes associated with membranes surrounding structures like cells, nuclei, and organelles. Consequently, as light propagates through inhomogeneous tissue, the phase delay introduced to different cross sectional areas of the beam can vary. These spatially varying shifts result in partial depolarization of the incident light upon combination in the focal plane. As the total number of refractive index changes scales with the thickness of tissue, it is expected that increasing thickness will result in increased depolarization induced by interaction with the sample. A DoP near 1 indicates a purely polarized field, while a DoP of zero corresponds to the limit of complete depolarization, (i.e., the only nonzero Stokes element is s_0). The mean DoP value for pixels used in polarization analysis in the measured samples shifted from 0.88 for 5 μm tissue, to 0.83 for 40 μm and 0.69 for 70 μm thickness. More striking, however, is the increased width in the distribution of recovered DoP values. Depolarization, as demonstrated here for the transmitted infrared beam, is not compatible the Jones calculus, requiring the more general Stokes framework.

While scattering and depolarization are a significant challenge in polarization analysis, they do not represent the only perturbation of polarization induced by the sample itself. Birefringence can also significantly alter the polarization of the fundamental, further complicating analysis. Figure 4 shows the change in polarization state $\Delta\vec{s} = \vec{s}_{\text{out}} - \vec{s}_{\text{in}}$ as a function of position, measured by taking the difference between the incident Stokes vector in regions without tissue with every pixel in the field of view. Δs_1, shown in parts A−C of Figure 4, highlights regions of linear rotation within the field of view while parts D−F of Figure 4 map Δs_3, corresponding to changes in ellipticity. In both the 40 and 70 μm tissue samples fibers diagonally aligned show significant birefringence relative to the rest of the field of view, particularly on regions near the edge of the tendon fibers. Scattering was also largest in these locations, as they represent regions within the field of view with significant heterogeneity in the refractive index. Both scattering and birefringence substantially increase as a function of tissue thickness.

This significant depolarization from propagation through the sectioned tissues prevents the direct use of Jones tensor analyses to recover tensor elements related to local structure, as the Jones architecture is only formally valid for purely polarized incident light. In the presence of depolarization, polarization states are more appropriately described by Stokes vectors. Measurement of the Stokes vectors of the fundamental and second harmonic fields is afforded by fitting to eq 7 while the mathematical relations given in eq 4 allow the more general Mueller tensor description of collagen to be fully described in terms of the simpler Jones tensor elements. Through this relation, incoming and exiting Stokes vectors describing partially polarized light can still be interpreted directly in terms of both the laboratory-frame Jones and local-frame Cartesian tensors normally reserved for purely polarized analyses, discussed here in the context of the tensor element ratio ρ.

DOI: 10.1021/acs.jpcb.9b04961
J. Phys. Chem. B 2019, 123, 6643−6650

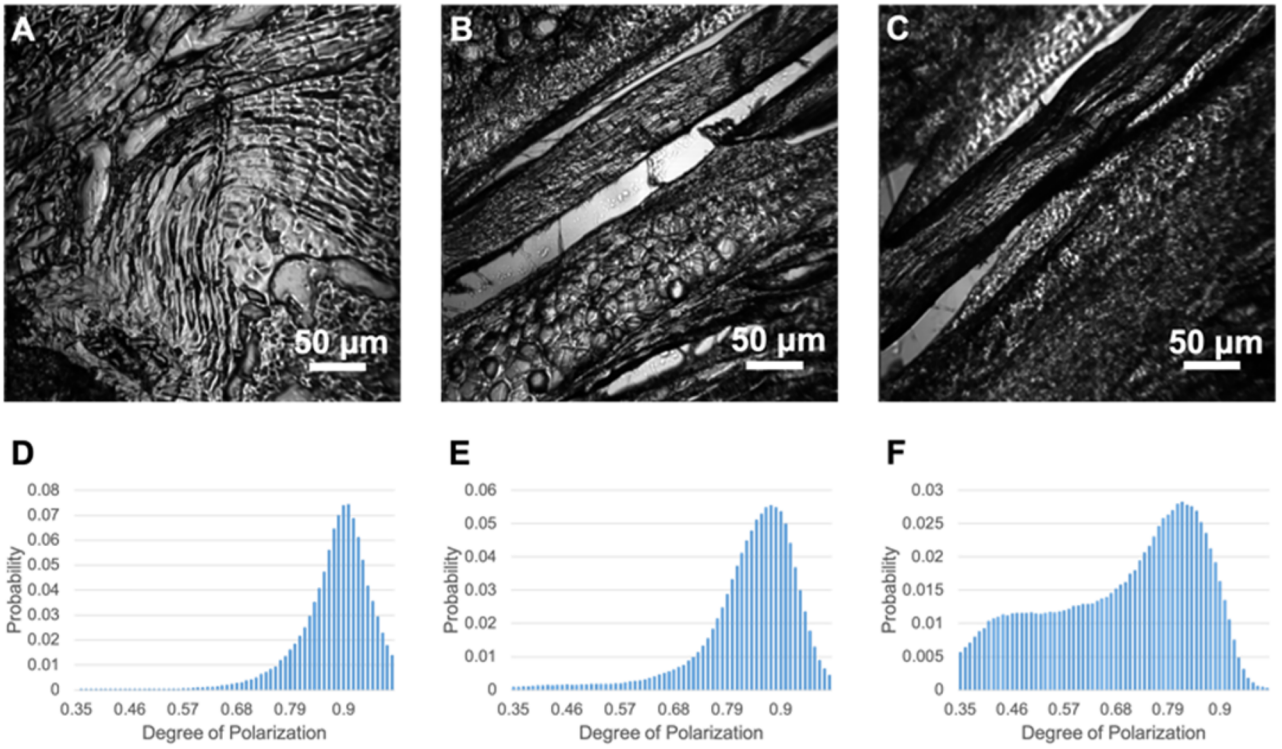

Figure 3. Laser transmittance images integrated across all polarizations and analyzer configurations for 5 (A), 40 (B), and 70 μm (C) thick tissue samples are displayed. Histograms of the degree of polarization for pixels used in polarization analysis are plotted, showing increased depolarization as a function of tissue thickness (D–F).

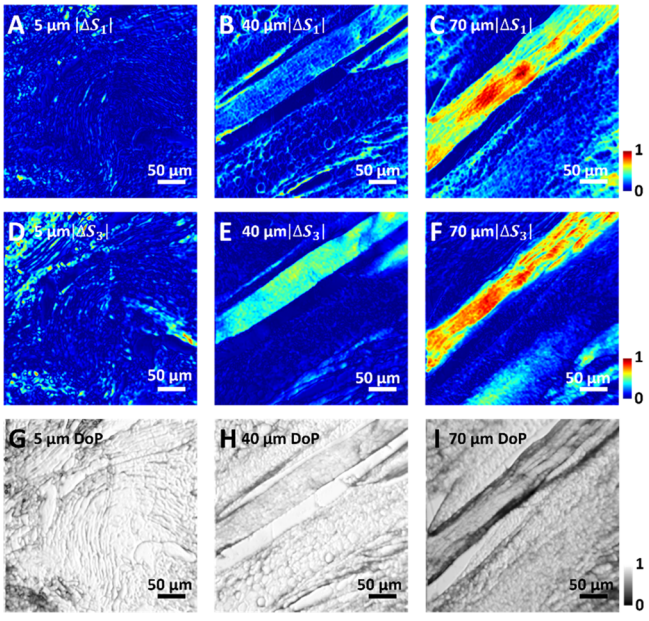

Figure 4. Images of the ΔS_1 (A–C) and ΔS_3 (D–F) vector elements for polarization state 1 of each tissue thickness show significant birefringence effects as a function of tissue thickness. The contrast is set from 0 to 1 in terms of absolute deviation, with blue representing 0 deviation from the reference blank and red a deviation of 1; the theoretical maximum deviation is 2. Maps of the DoP for the same polarization (G–I) show regions of high scattering occur preferentially near structural edges.

Nonlinear optical susceptibility tensor elements of collagen were imaged utilizing Stokes vectors obtained via linear fitting for both laser transmittance and bright field images. For collagen, the only unique nonzero local frame tensor elements by symmetry are χ_{zzz}, χ_{zxx}, χ_{xxz}, and χ_{yzx}, defined in a reference frame with the C_∞ fiber axis of collagen paralleling z. The chiral element χ_{yzx} is relatively small in magnitude and does not contribute to the detected intensity for collagen fibers aligned in the image plane within the paraxial approximation.[21] Quantum chemical calculations show the tropocollagen molecular hyperpolarizability is dominated by the β_{zzz} element.[22,23] Interchangeability of indices within the dominant β_{zzz} element at the molecular level translates to interchangeability at the ensemble level, such that projections of β_{zzz} onto the macromolecular elements χ_{zxx} and χ_{xxz} are identical. Experimentally, the approximate equality is often observed.[24] Using the assumption of equality for these two elements, the number of unknowns for the sample drops to 3: orientation, χ_{zxx}, and χ_{zzz}. Using the image analysis plugin OrientationJ for NIH ImageJ, local orientation of fibers can be extracted from the SHG images.[25,26] A nonlinear optimization to the tensor elements χ_{zzz} and χ_{zxx} using eqs 4–5 was conducted using the Levenberg–Marquardt algorithm.[27,28] The tensor element ratio ρ was then recovered, which has been used to analyze the local distribution of tilt angle of collagen fibrils about the fiber axis.[29,30]

It is interesting to compare the present results with previous measurements of SHG of collagen tissue obtained with fully depolarized incident light, prepared using a microretarder array depolarizer.[19] In that work, the NLO response was used to directly fit azimuthal and polar orientation of collagen, yielding good agreement between image analysis approaches and direct fitting to the azimuthal orientation angle of collagen. Given the established agreement between single-pixel polarization analysis and image texture analysis for quantifying collagen azimuthal orientation, a greater emphasis was placed here on

DOI: 10.1021/acs.jpcb.9b04961
J. Phys. Chem. B 2019, 123, 6643–6650

recovery of nonlinear optical parameters inaccessible from knowledge of azimuthal angle alone. Utilizing OrientationJ for azimuthal angle determination enabled increased statistical confidence in the nonlinear optical parameters recovered by fitting of the polarization-dependent SHG produced by partially polarized incident light.

Figure 5 shows orientation maps and colormaps of the χ_{zzz} and χ_{zxx} tensor elements for tissues of 5, 40, and 70 μm

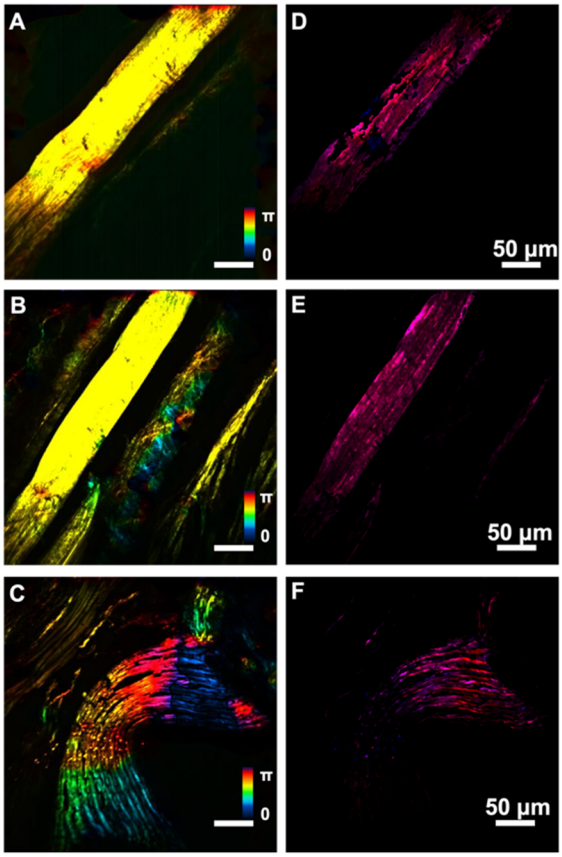

Figure 5. Orientation maps (A–C) and red-blue colormaps of χ_{zzz} and χ_{zxx} (D–F), for 70, 40, and 5 μm thick tissues obtained from the analysis.

thickness. Quantitative analysis of NLO susceptibility tensor elements was conducted for pixels containing less than 20% relative error in both coefficients, as determined by the Jacobian approximation to the Hessian in combination with the standard error of the fit. Pixels with negative ρ values were assumed to be nonphysical and excluded from this analysis; simulations suggest that Poisson noise in the shot-noise limited photomultiplier tube detector is sufficient to produce distributions in ρ with significant negative valued elements. Mean tensor ratios of 1.8, 1.8, and 2.3 were observed for the three tissue thicknesses. It is posited that the larger ρ value observed for the 70 μm tissue is due to the lower signal-to-noise ratio for that experiment. Indeed, Figure 5D shows large regions of SHG activity that produce fitted tensor values with high relative error, indicated by dark regions within the body of the fiber, and were thus excluded from analysis of the ρ distribution.

Most intriguing about the method of analysis utilized here is the ability to analyze the change in polarization induced by the process of SHG. As SHG is often mathematically treated as arising from only the purely polarized component of incident light, the effects of the SHG process on the overall degree of polarization of the exiting field is often neglected. Examination of the distributions of DoP for both the second harmonic and the infrared light indicates that the SHG was more polarized for 40 and 70 μm thick tissues than the corresponding pixels in the laser transmittance image, with ratios averaging 1.03 and 1.10 respectively. In contrast, the Stokes vectors of SHG in the thinnest tissue segment showed the greatest induced depolarization with a ratio of 0.82.

The observation of hyperpolarization from SHG measurements of collagen with partially depolarized incident light is consistent with previous studies of SHG produced from the limit of complete depolarization of the fundamental beam.[19] It has previously been shown that depolarized light incident to thin sections of collagenous tissue results in emission of partially polarized light, in excellent agreement with predictions from the Mueller tensor framework. The depolarized field is projected onto the finite set of nonzero tensor elements of the NLO susceptibility, which limits the potential polarization states of SHG. Consequently, the Stokes vector for SHG produced by collagen from a depolarized field always has a DoP_{SHG}/DoP_{IR} greater than one. This effect is qualitatively similar to fluorescence excitation with unpolarized light resulting in emitted light partially polarized parallel with the transition moment. This intrinsic hyperpolarization propensity in part may explain the increase in DoP_{SHG}/DoP_{IR} as tissue thickness increases, due to a larger relative contribution of depolarized incident light to stimulate SHG. If the histograms within parts E and F of Figure 3 are examined, the greatest mean in incident degree of polarization is observed for the thinnest tissue section. Similarly, parts G–I of Figure 4 show the greatest degree of polarization as a function of position, interpretable via the brightness in the images, for the thinnest tissue. For a fixed degree of depolarization inherent in the process of SHG from finite-sized objects, the relative polarization purity DoP_{SHG}/DoP_{IR} is smaller for the thin section, as the denominator is higher. Consequently, as the DoP_{IR} approaches zero, the hyperpolarization asymptotically approaches infinity.

In practice, this limiting case of complete depolarization of the incident beam is tempered by the presence of contributions from the purely polarized component of light as well, the interplay of which is dependent on the orientation of collagen. In the limit of no depolarization, the ratio of DoP_{SHG}/DoP_{IR} will simply be unity. The anticipated trends for partially polarized incident light relative to these two limits are not immediately obvious. Simulations of the DoP_{SHG}/DoP_{IR} as a function of orientation angle of collagen were performed to provide additional insights into the origin of the hyperpolarizing and depolarizing effects of SHG. Values of ρ = 1.8 and θ = 0 were assumed. Figure 6, shows a plot of DoP_{SHG}/DoP_{IR}, with a DoP_{IR} of 0.8, for H and V polarized light, right circularly polarized light, and left circularly polarized light. Light unperturbed by the sample can be interpreted in terms of these four components since measurements conducted modulated retardance of light incident to the tissue sample from a starting polarization of pure H light. For linearly polarized light the process of SHG under these conditions produces a Stokes vector that is either more or less purely polarized than the incident IR, as a function of collagen orientation. Circularly polarized incident light always produces

DOI: 10.1021/acs.jpcb.9b04961
J. Phys. Chem. B 2019, 123, 6643–6650

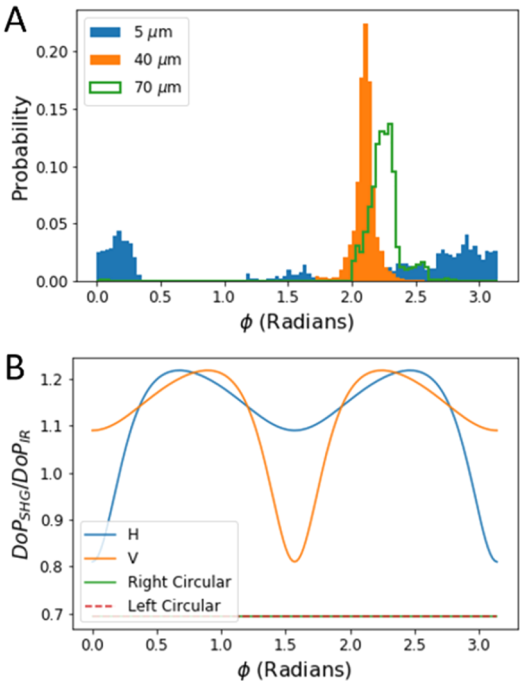

Figure 6. Distributions of orientation for 5, 40, and 70 μm thick tissue (A) are plotted. The simulated ratio of DoP_{SHG}/DoP_{IR}, as a function of collagen rotation in the plane (B) shows the SHG process to be either hyperpolarizing or depolarizing depending on orientation for linearly polarized light, and always to be depolarizing for circularly polarized light at DoP_{IR} = 0.8.

a relatively depolarized SHG field under the simulation conditions.

Physically, the maxima observed in Figure 6B can be explained by a competing relative contribution of partially polarized and fully polarized incident light to the total SHG intensity produced by the collagen fiber. The SHG produced can be considered as a linear combination of SHG occurring from depolarized and purely polarized incident light. Within this model, as the collagen fiber is rotated off of the axis of polarization of the incident field, the polarization of the SHG emitted from the purely polarized component is rotated. This has a secondary effect of modulating the intensity of the SHG emitted from the purely polarized component, due to the difference in tensor element magnitudes. Similarly, SHG from the depolarized fundamental beam component results in a partially polarized Stokes vector emitted by the collagen. This partially polarized Stokes vector rotates as a function of collagen orientation with respect to the laboratory frame, but at a constant intensity. The net effect is that the relative contribution of purely polarized light to SHG and relative contribution of depolarized light to the SHG are both changing, and there is a single collagen orientation for a given DoP_{IR}, which then maximally polarizes the output SHG.

These same collective arguments provide a potential explanation for the observation of a $DoP_{SHG}/DoP_{IR} < 1$ for the thinnest tissue section. Even through just 5 μm of tissue, the measured DoP_{IR} had a mean of 0.88, corresponding to small but non-negligible depolarization of the incident beam. The orientation distribution of collagen within the 5 μm thick tissue section suggests the origin of net depolarization via SHG when contrasted with the H-polarized intensity trace observed in Figure 6B. In Figure 6A, note the large population of orientations for the thin section near $\phi = 0$ and π, where SHG is maximally depolarizing for *H*-polarized incident light. In contrast, the same incident polarization becomes hyperpolarizing for collagen orientations near $\pi/4$ and $3\pi/4$ azimuthal angles, consistent with maxima in the orientation distributions of collagen in the 40 and 70 μm thick sections. This simplified model provides a qualitative explanation for the observed differences in depolarization and hyperpolarization for the different samples investigated.

CONCLUSION

A method was demonstrated for the experimental recovery of local frame tensor elements determining the NLO activity of collagen embedded in tissue. The method relies on the independent measurement of the Stokes vectors for the fundamental frequency and second harmonic beams, followed by fitting to recover the underlying Jones tensor elements. The distribution of the tensor element ratio ρ for collagen fibers in mouse tail tissue was measured, with mean tensor values of 1.8, 1.8, and 2.3 for 5, 40, and 70 μm samples, respectively, consistent with previous measurements of mouse tail sectioned thinly as well as previously reported values in the literature.[19,23,24] Recovery of consistent tensor element values for varying tissue thicknesses demonstrates utility of the Stokes–Mueller framework to account for changes in polarization from both birefringent and scattering effects on the fundamental frequency. The framework utilized leverages the simplicity of the Jones description for interpreting polarization dependent NLO with the general applicability of the Stokes description of polarization. Furthermore, this framework enables modification of existing architectures for analysis of NLO polarization to account for loss of polarization purity in the fundamental fields. Hyperpolarizing and depolarizing effects of SHG were observed, and their physical origin was ascribed to an interplay of the relative intensity contribution of polarized and depolarized light incident to the sample. The process of SHG is not often discussed in reference to its capacity to hyperpolarize or depolarize a field, and the observations reported herein are consequently of particular note.

AUTHOR INFORMATION

Corresponding Author

*(G.J.S.) E-mail: gsimpson@purdue.edu.

ORCID

Garth J. Simpson: 0000-0002-3932-848X

Notes

The authors declare no competing financial interest.

ACKNOWLEDGMENTS

The authors graciously acknowledge financial support from the National Science Foundation grant numbers 1710475 and 1763896 and National Institutes of Health grant 5R01GM103401 through the National Institute of General Medical Sciences.

REFERENCES

(1) Drobizhev, M.; Makarov, N. S.; Tillo, S. E.; Hughes, T. E.; Rebane, A. Two-Photon Absorption Properties of Fluorescent Proteins. *Nat. Methods* **2011**, *8* (5), 393–399.

(2) Yang, W.; Yuste, R. In Vivo Imaging of Neural Activity. *Nat. Methods* **2017**, *14*, 349.

DOI: 10.1021/acs.jpcb.9b04961
J. Phys. Chem. B 2019, 123, 6643–6650

(3) Li, D.; Zheng, W.; Zeng, Y.; Luo, Y.; Qu, J. Y. Two-Photon Excited Hemoglobin Fluorescence Provides Contrast Mechanism for Label-Free Imaging of Microvasculature in Vivo. *Opt. Lett.* **2011**, *36* (6), 834−836.
(4) Balu, M.; Mazhar, A.; Hayakawa, C. K.; Mittal, R.; Krasieva, T. B.; König, K.; Venugopalan, V.; Tromberg, B. J. In Vivo Multiphoton NADH Fluorescence Reveals Depth-Dependent Keratinocyte Metabolism in Human Skin. *Biophys. J.* **2013**, *104* (1), 258−267.
(5) Tilbury, K.; Lien, C.-H. H.; Chen, S.-J. J.; Campagnola, P. J. Differentiation of Col I and Col III Isoforms in Stromal Models of Ovarian Cancer by Analysis of Second Harmonic Generation Polarization and Emission Directionality. *Biophys. J.* **2014**, *106* (2), 354−365.
(6) Golaraei, A.; Cisek, R.; Krouglov, S.; Navab, R.; Niu, C.; Sakashita, S.; Yasufuku, K.; Tsao, M.-S.; Wilson, B. C.; Barzda, V. Characterization of Collagen in Non-Small Cell Lung Carcinoma with Second Harmonic Polarization Microscopy. *Biomed. Opt. Express* **2014**, *5* (10), 3562.
(7) Levental, K.; Yu, H.; Kass, L.; Lakins, J.; Egeblad, M.; et al. Matrix Crosslinking Forces Tumor Progression by Enhancing Integrin Signaling. *Cell* **2009**, *139* (5), 891−906.
(8) Kerian, Emma L. *Polarization-Dependent Nonlinear Optical Microscopy Methods for the Analysis of Crystals and Biological Tissues*. Ph.D. Dissertation, Purdue University, 2015.
(9) Roth, S.; Freund, I. Second Harmonic Generation in Collagen. *J. Chem. Phys.* **1979**, *70* (4), 1637−1643.
(10) Plotnikov, S. V.; Millard, A. C.; Campagnola, P. J.; Mohler, W. A. Characterization of the Myosin-Based Source for Second-Harmonic Generation from Muscle Sarcomeres. *Biophys. J.* **2006**, *90* (2), 693−703.
(11) Nadiarnykh, O.; Plotnikov, S.; Mohler, W. A.; Kalajzic, I.; Redford-Badwal, D.; Campagnola, P. J. Second Harmonic Generation Imaging Microscopy Studies of Osteogenesis Imperfecta. *J. Biomed. Opt.* **2007**, *12* (5), 051805.
(12) Gusachenko, I.; Latour, G.; Schanne-Klein, M.-C. Polarization-Resolved Second Harmonic Microscopy in Anisotropic Thick Tissues. *Opt. Express* **2010**, *18*, 19339−19352.
(13) de Aguiar, H.; Gigan, S.; Brasselet, S. Polarization Recovery through Scattering Media. *Sci. Adv.* **2017**, *3* (9), No. e1600743.
(14) Shi, Y.; McClain, W.M.; Harris, R.A. physics letters, H.-R. An Extension of the Mueller Scattering Matrix to Nonlinear Light Scattering. *Chem. Phys. Lett.* **1993**, *205* (1), 91−95.
(15) Shi, Y.; McClain, W. M.; Harris, R. A. Generalized Stokes−Mueller Formalism for Two-Photon Absorption, Frequency Doubling, and Hyper-Raman Scattering. *Phys. Rev. A: At., Mol., Opt. Phys.* **1994**, *49* (3), 1999−2015.
(16) Samim, M.; Krouglov, S.; Barzda, V. Double Stokes Mueller Polarimetry of Second-Harmonic Generation in Ordered Molecular Structures. *J. Opt. Soc. Am. B* **2015**, *32* (3), 451−461.
(17) Burke, M.; Golaraei, A.; Atkins, A.; et al. structural biology, A.-M. Collagen Fibril Organization within Rat Vertebral Bone Modified with Metastatic Involvement. *J. Struct. Biol.* **2017**, *199* (2), 153−164.
(18) Simpson, G. Connection of Jones and Mueller Tensors in Second Harmonic Generation and Multi-Photon Fluorescence Measurements. *J. Phys. Chem. B* **2016**, *120* (13), 3281−3302.
(19) Ding, C.; Ulcickas, J. R. W.; Deng, F.; Simpson, G. J. Second Harmonic Generation of Unpolarized Light. *Phys. Rev. Lett.* **2017**, *119* (19), 193901.
(20) DeWalt, E. L.; Sullivan, S. Z.; Schmitt, P. D.; Muir, R. D.; Simpson, G. J. Polarization-Modulated Second Harmonic Generation Ellipsometric Microscopy at Video Rate. *Anal. Chem.* **2014**, *86* (16), 8448−8456.
(21) Dow, X. Y.; DeWalt, E. L.; Sullivan, S. Z.; Schmitt, P. D.; Ulcickas, J. R. W.; Simpson, G. J. Imaging the Nonlinear Susceptibility Tensor of Collagen by Nonlinear Optical Stokes Ellipsometry. *Biophys. J.* **2016**, *111* (7), 1361−1374.
(22) de Wergifosse, M.; de Ruyck, J.; Champagne, B. How the Second-Order Nonlinear Optical Response of the Collagen Triple Helix Appears: A Theoretical Investigation. *J. Phys. Chem. C* **2014**, *118* (16), 8595−8602.
(23) Dow, X. Y.; DeWalt, E.; Sullivan, S. Z.; Schmitt, P. D.; Ulcickas, J.; Simpson, G. J. Imaging the Nonlinear Susceptibility Tensor of Collagen by Nonlinear Optical Stokes Ellipsometry. *Biophys. J.* **2016**, *111* (7), 1361.
(24) Romijn, E.; Finnøy, A.; Lilledahl, M. B. Analyzing the Feasibility of Discriminating between Collagen Type I and II Using Polarization Resolved Second Harmonic Generation. *J. Biophot.* **2019**, *12* (1), No. e201800090.
(25) Schneider, C. A; Rasband, W. S; Eliceiri, K. W NIH Image to ImageJ: 25 Years of Image Analysis. *Nat. Methods* **2012**, *9* (7), 671−675.
(26) Rezakhaniha, R.; Agianniotis, A.; et al. modeling in··· J. Experimental Investigation of Collagen Waviness and Orientation in the Arterial Adventitia Using Confocal Laser Scanning Microscopy. *Biomech. Model. Mechanobiol.* **2012**, *11* (3-4), 461−473.
(27) Levenberg, K. A method for the solution of certain non-linear problems in least squares. *Q. Appl. Math.* **1944**, *2* (2), 164−168.
(28) Marquardt, D. W. An Algorithm for Least-Squares Estimation of Nonlinear Parameters. *J. Soc. Ind. Appl. Math.* **1963**, *11* (2), 431−441.
(29) Su, P.-J.; Chen, W.-L.; Hong, J.-B.; Li, T.-H.; Wu, R.-J.; Chou, C.-K.; Chen, S.-J.; Hu, C.; Lin, S.-J.; Dong, C.-Y. Discrimination of Collagen in Normal and Pathological Skin Dermis through Second-Order Susceptibility Microscopy. *Opt. Express* **2009**, *17* (13), 11161−11171.
(30) Chen, W.-L.; Li, T.-H.; Su, P.-J.; Chou, C.-K.; Fwu, P. T.; Lin, S.-J.; Kim, D.; So, P. T. C.; Dong, C.-Y. Second Harmonic Generation χ Tensor Microscopy for Tissue Imaging. *Appl. Phys. Lett.* **2009**, *94* (18), 183902.

DOI: 10.1021/acs.jpcb.9b04961
J. Phys. Chem. B 2019, 123, 6643−6650